One-dimensional physics in transition-metal nanowires: Renormalization group and bosonization analysis

Jun-ichi Okamoto and A. J. Millis

One-dimensional physics in transition-metal nanowires: Renormalization group and bosonization analysis

Jun-ichi Okamoto[*] and A. J. Millis[†]

Department of Physics, Columbia University, 538 West 120th Street, New York, New York 10027, USA

(Dated: February 1, 2012)

We study the one-dimensional two-orbital Hubbard model with general local interactions including a pair-hopping term. The model might be realized in one-dimensional transition-metal nanowires. Phase diagrams at $T = 0$ are obtained by numerical integration of renormalization group equations and bosonization. Particular attention is paid to the effects of orbital degeneracy (or near-degeneracy), interactions favoring locally high-spin configurations, and velocity differences. Dynamical symmetry enlargement and duality approaches are employed to determine ground states and to understand quantum phase transitions between them. An important result is that the pair-hopping term and associated orbital symmetry can lead to new insulating states. The ground state for spin-polarized case is also discussed.

I. INTRODUCTION

Theoretical models involving two orbitals per unit cell in one dimension have been employed to understand various strongly correlated systems ,e.g., heavy fermion compounds,[1–3] high-T_c superconductors,[4–12] spin-ladders,[13,14] and Hubbard-ladders.[15–17] These models are often referred to as "ladder models" because one may visualize the two states as opposite sides of a rung. Recent experiments demonstrate the formation of self-assembled transition-metal nanowires, adding another possible realization of ladder models.[18,19] In such systems, one-dimensional (1D) nanowires composed of transition-metal atoms are confined at step edges on a substrate surface. In many physically relevant cases, the surface bandgap structure of the substrate material is such that the electronic states of the adatoms are decoupled from the bulk substrate bands (at least to leading order and for low energies) and the d-orbital bands derived from the transition-metal nanowire form a multi-component one-dimensional Fermi gas with variety of interactions. Classifying the kinds of behavior which may be observed in these systems is an important open question. In this paper, we will focus on the case where only two bands cross the Fermi energy. This situation is equivalent to two-leg ladder models, which have been previously studied.

Past studies revealed that two-leg ladder systems may exhibit dynamical symmetry enlargement (DSE)[10,20,21] and dualities among ground states.[22–24] DSE occurs when a RG flow leads to an effective low energy fixed point which exhibits a higher symmetry than that of original lattice Hamiltonian. In two-leg ladder models, the emergent symmetry is known to be O(6)×U(1) when the system is away from half filling, and O(8) at half filling. The different ground states of these low-energy theories are related to each other by duality mappings, which are generalizations of the Kramers-Wannier duality seen in the two dimensional Ising model.[25]

We expect that many qualitative aspects of two-leg ladder models, including DSE and duality properties, hold also in our models of transition-metal nanowires. However, new features of transition-metal wires require additional investigation. The orbital degeneracy of the transition-metal d-levels permits a rich set of onsite Coulomb interactions. In particular, the Hund coupling favors locally high spin configurations, and we speculate that the ground states may exhibit non-zero spin structure. Furthermore, the pair-hopping term, which has been neglected in some previous studies, is found to be important; it implies the system has a unique orbital symmetry. We generically expect that orbital symmetry breaking at the level of the one-body terms leads to velocity differences between different orbitals. A large velocity difference complicates the application of established methods such as refermionization[26] to our model. Strong correlation may also lead to spin-polarized states or to ferromagnetism observed, for example, in Co nanowires.[27] Finally, the possible realization of an orbital selective Mott phase[28] in one-dimension is an open issue.

In order to understand the effect of these features of transition-metal nanowires, we study the one-dimensional two-orbital Hubbard model using perturbative renormalization group (RG) and bosonization approaches. We combine the ideas of DSE and duality to list the possible ground states of our models. We find the form of interaction relevant to transition-metal d-levels leads to a new group of eight insulating phases when the two orbitals are completely degenerate. We then obtain ground state phase diagrams using RG and bosonization. In physically relevant parameter regimes, the stability of the ground states to velocity differences is also investigated. To be complete, the fully spin-polarized case, where the model is reduced to a Hubbard model with or without magnetic field, is also briefly analyzed.

The methods we employ in this paper are strictly applicable when the system is truly one-dimensional, and the interaction is weak. Our results are complimentary to those we previously obtained for same model using

mean-field approaches.[29] The present results allow more complete understanding of the weak-coupling regime, but the mean-field theory can treat the intermediate and strong coupling regimes.

The organization of this paper is as follows. In Sec. II we explain the model and approximation we employed. In Sec. III, we derive bosonized forms of the model. Section IV is devoted to explanation of various possible order parameters. In section V, we use the idea of dynamical symmetry enlargement and duality to understand the relations among ground states. Quantum phase transitions among these ground states are explained. In section VI, RG equations and obtained phase diagrams are shown. The fully-spin polarized case is briefly discussed in Sec. VII. Finally, Sec. VIII is a conclusion and summary.

II. MODEL

We start from a multi-orbital Hubbard model representing the transition-metal d-orbitals with local on-site Coulomb interactions

$$H = \sum_{\langle i,j \rangle} \sum_{m,s} -t_{ij}^{mm'} \left(c_{ims}^\dagger c_{jm's} + \text{h.c.} \right) + H_{\text{int}}. \quad (1)$$

Here $c_{ims}^{(\dagger)}$ is the annihilation (creation) operator for a d-electron in orbital m with spin s at site i. $t_{ij}^{mm'}$ is the hopping between from orbital m on site i to orbital m' on site j. The interaction terms H_{int} will be shown below. We believe this model encapsulates the physics of transition-metal nanowires. Through the paper, we set the lattice constant to unity. A symmetry breaking field occurs due to the one-dimensional geometry, and the presence of the substrate may further lift the degeneracy of orbitals as well as providing an arbitrary ionization level. Thus, in a general case, one may have many d-derived bands with an arbitrary Fermi energy.

For the sake of simplicity, we will consider here only the cases where two orbitals, A and B, are present at the Fermi level. The rotational symmetry in H_{int} as we will see always allows us to diagonalize the hopping matrix, so we will ignore off-diagonal terms in the hopping. The band structure is then characterized by four Fermi points: two Fermi momenta, k_A and k_B, and two chiralities $r = R, L$, representing electrons around the positive (R) and negative (L) Fermi momentum. The total particle number is $n = 2(k_A + k_B)/\pi$. In principle there are five possible cases which are summarized in Table I. In cases (a) and (b), the two Fermi momenta are equal, and the filling is commensurate and incommensurate respectively. In cases (c) and (d), the two Fermi momenta are different, while (c) is at half filling, and (d) is away from half filling. Finally in case (e), one band is commensurate and the other is not, allowing an orbital selective Mott state.

For the two-orbital system the interaction terms have

the following form:

$$\begin{aligned}
H_{\text{int}} = &U \sum_{i,m} n_{im\uparrow} n_{im\downarrow} \\
&+ U' \sum_{i,s} n_{iAs} n_{iB\bar{s}} \\
&+ (U' - J) \sum_{i,s} n_{iAs} n_{iBs} \\
&- J \sum_{i,s,} c_{iAs}^\dagger c_{iA\bar{s}} c_{iB\bar{s}}^\dagger c_{iBs} \\
&+ J' \sum_{i,m} c_{im\uparrow}^\dagger c_{im\downarrow}^\dagger c_{i\bar{m}\downarrow} c_{i\bar{m}\uparrow},
\end{aligned} \quad (2)$$

where and $n_{ims} = c_{ims}^\dagger c_{ims}$ is the electron density. $\bar{s} = -s$ and $\bar{m}$ means $B(A)$ if $m = A(B)$. Since the substrate will screen the long-ranged Coulomb interaction, we include only on-site Coulomb interactions. U and U' indicates on-site Coulomb repulsion between two electrons in the same band or different bands, and J represents the Hund coupling favoring high spin states. J' is the so called pair-hopping term. For a transition-metal ion in free space all of these parameters are positive. Now, we assume the following relationship among them, which is usually preserved among d-orbitals,

$$J' = J \quad (3)$$
$$U' = U - 2J. \quad (4)$$

To make the symmetry of the interaction terms explicit, we introduce the following charge, spin, and orbital (pseudo-spin) operators:

$$n_i = \sum_{ms} n_{ims}, \quad (5)$$

$$\boldsymbol{S}_i = \frac{1}{2} \sum_{mss'} c_{ims}^\dagger \boldsymbol{\sigma}_{ss'} c_{ims'}, \quad (6)$$

$$\boldsymbol{T}_i = \frac{1}{2} \sum_{mm's} c_{ims}^\dagger \boldsymbol{\tau}_{mm'} c_{im's}, \quad (7)$$

where $\boldsymbol{\sigma}$ and $\boldsymbol{\tau}$ are Pauli matrices. Then, the interactions in terms of U and J are given by,

$$H_{\text{int}} = \sum_i \left(\frac{U}{2} n_i^2 + J\boldsymbol{S}_i^2 + 3J\boldsymbol{T}_i^2 - 2J(T_i^y)^2 - \frac{U+5J}{2} n_i \right). \quad (8)$$

Since $U' > 0$, the physically relevant range of J is limited to $0 < J < U/2$.

Now we discuss the symmetry of our Hamiltonian at the bare level. When $J = 0$, the interaction term possesses $U(1)_c \times SU(4)_{s,o} \times \mathcal{Z}_2$; the indices "c", "s", and "o" denote the charge, spin and orbital parts, and the $\mathcal{Z}_2$ symmetry refers to the interchange of orbitals. When $J \neq 0$, the symmetry of the spin-orbital part is broken to $SU(2)_s \times U(1)_o$. We'd like to emphasize that in our convention, the $U(1)$ axis is the orbital y-axis, wheres

TABLE I. Possible band structures in the two-orbital Hubbard model, and its symmetries when $v_A = v_B$. $U(1)_r$ represents a gauge transformation of particles with chirality r.

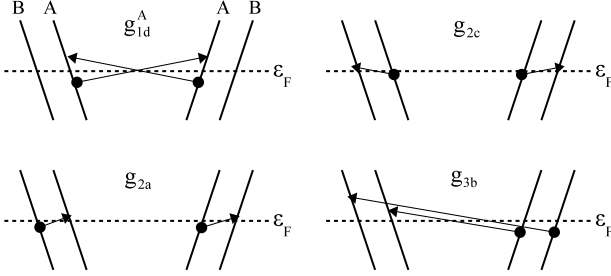| Case	Fermi momentum	n	symmetries
(a)	$k_A = k_B$	$= 2$	$U(1)_c \times SU(2)_s \times U(1)_o \times \mathcal{Z}_2$
(b)	$k_A = k_B$	$\neq 2$	$U(1)_R \times U(1)_L \times SU(2)_s \times U(1)_o \times \mathcal{Z}_2$
(c)	$k_A \neq k_B$	$= 2$	$U(1)_c \times SU(2)_s \times \widetilde{U(1)}_o$
(d)	$k_A \neq k_B$	$\neq 2$	$U(1)_R \times U(1)_L \times SU(2)_s \times \widetilde{U(1)}_o$
(e)	$k_A \neq k_B = \pi/2$	$\neq 2$	$U(1)_c \times SU(2)_s \times \widetilde{U(1)}_o$

FIG. 1. Various scattering processes and "g-ology"

it is orbital z-axis in the convention of Refs. 24 and 30. Only if $v_A = v_B$ and $k_A = k_B$, as in cases (a) and (b), does the total Hamiltonian have the same symmetry as the interaction. Otherwise, including cases (c)–(e), the total symmetry is reduced to $U(1)_c \times SU(2)_s$ at the bare level due to the lower symmetry of the kinetic term. However, it is known that low-energy theories in weak-coupling still have an effective $\widetilde{U(1)}_o$ symmetry[10,21,23,24] at least if $v_A = v_B$. We will see this in detail later.

III. BOSONIZATION

In 1D systems, it is known that bosonization enables us to describe the low energy physics in a simple manner. In this section we present an Abelian-bosonization analysis, which is useful for the cases when difference in velocities is negligible. Appendix B outlines the more complicated formalism needed for unequal velocities.

To classify the various scattering processes we follow the notation of Ref. 12. "1–4" corresponds to conventional "g-ology" indices for left and right moving fields, and "a–d" are similar but label orbital indices. Some examples are given in Fig. 1. The $SU(2)_s$ symmetry constrains coupling constants as

$$g_{1d}^m - g_{2d}^m = 0$$
$$g_{2b}^\perp - g_{2b}^\parallel - g_{1a} = 0 \qquad (9)$$
$$g_{1c} - g_{2c} + g_{\parallel c} = 0.$$

For the rest of the paper, we will omit $\perp$ when it is not confusing.

When two Fermi points coincide, we have additional processes $g_{\parallel a}$, g_{1b}, and g_{2a}, which are connected by the $SU(2)_s$ symmetry as,

$$g_{\parallel a} - g_{1b} + g_{2a} = 0. \qquad (10)$$

$k_A = k_B$ means that we have the $U(1)_o$ symmetry, and this implies

$$g_{1(2)d}^A - g_{1(2)d}^B = 0$$
$$-g_{2d}^m + g_{2b}^\perp + g_{2c} + g_{2a} = 0$$
$$-g_{1d}^m + g_{1b} + g_{1c} + g_{1a} = 0 \qquad (11)$$
$$g_{2b}^\parallel + g_{\parallel c} - g_{\parallel a} = 0.$$

As Umklapp processes, we have $g_{\parallel b}$ and g_{3i} ($i = a–d$). The g_{3d}^m process represents the intraband Umklapp process, so it only exists for $k_m = \pi/2$. Other Umklapp processes are possible whenever $n = 2$. The $SU(2)_s$ symmetry gives

$$g_{3a} + g_{\parallel b} - g_{3b} = 0, \qquad (12)$$

and the $U(1)_o$ symmetry leaves

$$g_{3d} = g_{3a} + g_{3b} + g_{3c}. \qquad (13)$$

Using the standard bosonization formalism,[31–33] the Hamiltonian density $\mathcal{H}_0$ of the free-boson part becomes,

$$\mathcal{H}_0 = \frac{1}{2\pi} \sum_{\substack{\mu=c,s \\ \nu=0,\pi}} v_{\mu\nu} \left[K_{\mu\nu}(\nabla\theta_{\mu\nu})^2 + \frac{1}{K_{\mu\nu}}(\nabla\phi_{\mu\nu})^2 \right] \quad (14)$$

where ϕ and θ are connected to density and current: $\nabla\phi \propto n$, and $\nabla\theta \propto j$. The renormalized Luttinger parameters and velocities are given by

$$K_{c0(\pi)} = \sqrt{\frac{1 - (y_{1d} \pm y_{2b})/2}{1 + (y_{1d} \pm y_{2b})/2}} \equiv 1 - y_{c0(\pi)}$$

$$K_{s0(\pi)} = \sqrt{\frac{1 + (y_{1d} \pm y_{1a})/2}{1 - (y_{1d} \pm y_{1a})/2}} \equiv 1 - y_{s0(\pi)} \qquad (15)$$

$$v_{c0(\pi)} = v\sqrt{1 - (y_{1d} \pm y_{2b})^2/4}$$

$$v_{s0(\pi)} = v\sqrt{1 - (y_{1d} \mp y_{1a})^2/4}$$

with $y_i \equiv g_i/4\pi v$ and $y_{2b} \equiv y_{2b}^\perp + y_{2b}^\parallel$. "$c$" and "$s$" represent the charge and spin modes, and "0" and "π" are

used for bonding and antibonding combination. We introduced $y_{\mu\nu}$ for each Luttinger parameter for later use. A detailed derivation of this Hamiltonian is given in Appendix A. We ignore the velocity difference induced by the g_4 process, since its effect is to shift the phase boundaries slightly. We will provide a separate treatment for systems in which difference of initial velocities is quite large.

The $SU(2)_s$ symmetry fixes $K_{s0(\pi)}$ to be

$$K_{s0(\pi)} = 1 + (y_{1d} \pm y_{1a})/2 \equiv 1 - y_{s0(\pi)} \qquad (16)$$

along the RG flow. Similarly the $U(1)_o$ symmetry (when it exists) constrains $K_{c\pi}$ to be

$$K_{c\pi} = 1 + (-y_{1d} + y_{2b})/2 \equiv 1 - y_{c\pi}. \qquad (17)$$

The interaction part of the Hamiltonian is rather complicated. The interaction terms common to all cases are

$$
\begin{aligned}
H_{\text{int}} = {}& g_{1d} \int \cos{(2\phi_{s0})} \cos{(2\phi_{s\pi})} \\
& + g_{1a} \int \cos{(2\phi_{s0})} \cos{(2\theta_{s\pi})} \\
& - g_{1c} \int \cos{(2\phi_{s0})} \cos{(2\theta_{c\pi})} \qquad (18) \\
& - g_{2c} \int \cos{(2\phi_{s\pi})} \cos{(2\theta_{c\pi})} \\
& + g_{\|c} \int \cos{(2\theta_{s\pi})} \cos{(2\theta_{c\pi})}.
\end{aligned}
$$

Here $\int$ stands for $(2\pi\alpha)^{-2} \int dx$, and α is the cut-off which is of the order of the lattice constant. The last term does not exist in the original Hamiltonian, but will be generated after the one-loop renormalization.

When $k_A = k_B$, in cases (a) and (b), additional processes are allowed,

$$
\begin{aligned}
H'_{\text{int}} = {}& g_{\|a} \int \cos{(2\phi_{s\pi})} \cos{(2\phi_{c\pi})} \\
& + g_{1b} \int \cos{(2\phi_{s0})} \cos{(2\phi_{c\pi})} \qquad (19) \\
& + g_{2a} \int \cos{(2\theta_{s\pi})} \cos{(2\phi_{c\pi})}.
\end{aligned}
$$

Finally when the filling is commensurate, we have

$$
\begin{aligned}
H''_{\text{int}} = {}& g_{3a} \int \cos{(2\phi_{c0})} \cos{(2\theta_{s\pi})} \\
& - g_{3b} \int \cos{(2\phi_{c0})} \cos{(2\phi_{s\pi})} \\
& - g_{3c} \int \cos{(2\phi_{c0})} \cos{(2\theta_{c\pi})} \qquad (20) \\
& - g_{3d} \int \cos{(2\phi_{c0})} \cos{(2\phi_{c\pi})} \\
& - g_{\|b} \int \cos{(2\phi_{c0})} \cos{(2\phi_{s0})}.
\end{aligned}
$$

The g_{3d} process exists only when both bands are commensurate, case (a). Again, we ignored the g_4 type interactions whose scaling dimension is always larger than two, and this is consistent with the equal velocity approximation. The initial values of these coupling constants are: $g_{1d} = g_{3d} = 4U$, $g_{1a} = g_{1c} = g_{2c} = g_{2a} = g_{3a} = g_{3c} = 4J$, $g_{2b}^{\|} = g_{\|a} = g_{\|b} = 4(U - 3J)$, and $g_{1b} = g_{2b}^{\perp} = g_{3b} = 4(U - 2J)$. They will take different values after renormalization.

Finally we will discuss the symmetry of the linearized model (Table I). First, $U(1)_c$ and $SU(2)_s$ (around z-axis) are displayed in the invariance of the Hamiltonian under the translation of θ_{c0} and θ_{s0}. In fermionic language, each corresponds to the following gauge transformation:

$$c_{rms} \to e^{i\alpha} c_{rms}, \quad c_{rms} \to e^{is\alpha} c_{rms}. \qquad (21)$$

The indices r, m, and s represent chirality, orbital, and spin, and α expresses the constant phase shift. The conserved Noether currents, corresponding to the $U(1)_c$ and $SU(2)_s$ symmetries are,

$$
\begin{aligned}
\sum_{rms} N_{rms} &\propto \int dx \nabla \phi_{c0}, \\
\sum_{rms} s N_{rms} &\propto \int dx \nabla \phi_{s0},
\end{aligned} \qquad (22)
$$

where N_{rms} is the particle number at the branch specified by r, m, and s. Since $\nabla \phi$ is momentum conjugate of θ, the operator $\exp{\left(\int dx \nabla \phi \right)}$ gives a constant shift of θ. The $SU(2)_s$ rotation around x- and y-axis are not manifest in Abelian bosonization.

Away from half filling, there is also a continuous chiral symmetry under the transformation, $c_{rms} \to e^{ir\alpha} c_{rms}$. Thus, the Hamiltonian is invariant under arbitrary translation of ϕ_{c0}, with conserved total currents, $J_A + J_B \propto \int dx \nabla \theta_{c0}$ where $J_m = \sum_s N_{Rms} - N_{Lms}$. At half filling, this symmetry is broken to a discrete symmetry, and true long-range order can be realized.[17] When a system has both the chiral symmetry and the $U(1)_c$ symmetry, this implies that left, and right moving parts have separate conservation laws corresponding to the $U(1)_R \times U(1)_L$ symmetry. Similarly, other gauge transformations such as

$$
\begin{aligned}
c_{rms} &\to e^{im\alpha} c_{rms} \\
c_{rms} &\to e^{ims\alpha} c_{rms} \\
c_{rms} &\to e^{irs\alpha} c_{rms} \qquad (23) \\
c_{rms} &\to e^{irms\alpha} c_{rms}
\end{aligned}
$$

leave the Hamiltonian invariant for discrete values of $\alpha = n\pi/2$; each corresponds to the discrete shift of $\theta_{c\pi}$, $\theta_{s\pi}$, ϕ_{s0}, and $\phi_{s\pi}$.

The effective $\widetilde{U(1)}_o$ symmetry appearing when $k_A \neq k_B$ and $v_A = v_B$,[10,21,23,24] corresponds to the invariance

under the translation of $\phi_{c\pi}$ or the gauge transformation,

$$c_{rms} \rightarrow e^{irm\alpha}c_{rms}. \qquad (24)$$

The conserved "charge" corresponding to this symmetry is the difference of two orbital currents: $J_A - J_B \propto \int dx \nabla \theta_{c\pi}$.

When $k_A = k_B$, there is an explicit orbital rotational symmetry about y-axis. This transformation mixes fermions in different orbitals, so its generator cannot be expressed as a local operator in Abelian bosonization. This fact leads to a new combination of possible ground states as will be shown.

IV. ORDER PARAMETERS

A. Order parameters away from half filling

As order parameters, we take fermion bilinears characterized by the chirality, spin and orbital indices; thus in the model considered here there are particle-hole bilinears,

$$(\Delta_{\text{ph}})_{rr'}^{ss';mm'} = c_{rms}^{\dagger}c_{r'm's'} \qquad (25)$$

and particle-particle bilinears,

$$(\Delta_{\text{pp}})_{rr'}^{ss';mm'} = ms c_{rms}^{\dagger}c_{\overline{r'm's'}}^{\dagger}, \qquad (26)$$

where $c_{ms}^{(\dagger)}$ is the annihilation (creation) operator of electron with chirality r, orbital m, and spin s. Since combinations of $r = r'$ are irrelevant in a RG sense, we will fix $(r, r') = (R, L)$ in the remainder of this paper. We will use the following convenient basis to represent them,

$$\mathcal{O}_{\text{ph}}^{ij} = \sum_{mm'ss'} \tau_{mm'}^{i}\sigma_{ss'}^{j}(\Delta_{\text{ph}})^{ss';mm'} + \text{h.c.} \qquad (27)$$

$$\mathcal{O}_{\text{pp}}^{ij} = \sum_{mm'ss'} \tau_{mm'}^{i}\sigma_{ss'}^{j}(\Delta_{\text{pp}})^{ss';mm'} + \text{h.c.} \qquad (28)$$

where $i, j = (0, 1, 2, 3)$ and τ and σ are Pauli matrices with $\tau_{ab}^0 = \sigma_{ab}^0 = \delta_{ab}$. These transform as rank 2 tensors under $\text{SO}(4) \simeq \text{SU}(2)_s \times \text{SU}(2)_o$ transformations; the $\text{SU}(2)_s$ rotations connect $\sigma^{1,2,3}$, and the $\text{U}(1)_o$ rotation (if it exists) connects τ^1 and τ^3. Thus, we take the quantization axis along z-direction for spins. Additionally, as we will show below, all the high spin states ($j = 3$) such as SDW states and triplet superconductivities are excluded from the possible ground states in our models, so we will not consider them.

We label our order parameters by the transferred momentum and the sign at each Fermi point. Here we have four Fermi points each degenerate about spins, so, in principle, there are four possible cases (Table II). We use s-wave when all four points have the same signs. p_x and p_y are odd under the inversion $R \leftrightarrow L$, and $A \leftrightarrow B$ respectively. d-wave is odd under both inversions.

TABLE II. Angular momentum and corresponding signs of an order parameter at each Fermi point

"Angular momentum"	(A, R)	(A, L)	(B, R)	(B, L)
s	$+$	$+$	$+$	$+$
p_x	$+$	$-$	$+$	$-$
p_y	$+$	$+$	$-$	$-$
d	$+$	$-$	$-$	$+$

Applying this classification, we find that $i = 0, 1$ are both s-wave for the particle-hole channel, while the former is intraband type and the latter is interband type. We put " $'$ " for an interband order to distinguish these two. $i = 2$ is found to be interband p_y-wave, and $i = 3$ is intraband p_y-wave. For the particle-particle channel, we found d'-, p_y-, s-, and s'-wave orders for $i = 0, \dots, 3$ accordingly. Since p_x-wave does not appear in this study, we will use p for p_y-wave orders in the rest of the paper. We note that the d-wave superconductivity, which often appears in two-leg ladder models,[8] is the $p\text{SS}$ state in our notation. The result is summarized in Table III.

The order parameters in bosonized forms are,

$$\begin{aligned}
\mathcal{O}_{\text{ph}}^{00} &\propto \cos(k_0 x - \phi_{c0})\sin(k_\pi x - \phi_{c\pi})\sin(\phi_{s0})\sin(\phi_{s\pi}) \\
\mathcal{O}_{\text{ph}}^{10} &\propto \cos(k_0 x - \phi_{c0})\sin(\theta_{c\pi})\cos(\phi_{s0})\cos(\theta_{s\pi}) \\
\mathcal{O}_{\text{ph}}^{20} &\propto \cos(k_0 x - \phi_{c0})\cos(\theta_{c\pi})\cos(\phi_{s0})\cos(\theta_{s\pi}) \\
\mathcal{O}_{\text{ph}}^{30} &\propto \cos(k_0 x - \phi_{c0})\sin(k_\pi x - \phi_{c\pi})\cos(\phi_{s0})\cos(\phi_{s\pi})
\end{aligned} \qquad (29)$$

$$\begin{aligned}
\mathcal{O}_{\text{pp}}^{00} &\propto e^{-i\theta_{c0}}\sin(k_\pi x - \phi_{c\pi})\cos(\phi_{s0})\cos(\theta_{s\pi}) \\
\mathcal{O}_{\text{pp}}^{10} &\propto e^{-i\theta_{c0}}\sin(\theta_{c\pi})\sin(\phi_{s0})\sin(\phi_{s\pi}) \\
\mathcal{O}_{\text{pp}}^{20} &\propto e^{-i\theta_{c0}}\cos(\theta_{c\pi})\sin(\phi_{s0})\sin(\phi_{s\pi}) \\
\mathcal{O}_{\text{pp}}^{30} &\propto e^{-i\theta_{c0}}\sin(k_\pi x - \phi_{c\pi})\sin(\phi_{s0})\sin(\theta_{s\pi}),
\end{aligned} \qquad (30)$$

with $k_{0(\pi)} = k_A \pm k_B$. If coupling constants grow to the order of t after renormalization, the corresponding bosonic fields are pinned to the values which minimize the resultant potential. For incommensurate fillings, the total charge mode is massless, and the interaction terms pin the other modes to definite values (in mod of π). The pinned values determine the order parameter which gives a finite value of correlation. It is easy to find such pinned values from the above expressions, e.g., $(\theta_{c\pi}, \phi_{s0}, \phi_{s\pi}) = (\pi/2, 0, 0)$ for the $s'\text{CDW}$ state.

B. Order parameters at half filling

When a filling is commensurate, insulating phases (with the gapped total charge mode) become possible, and it turns out that the generic behavior is either that all fields are massless or all fields are gapped. We discuss the fully gapped phases here. In the bosonized representation, the physics is described by the conjugate fields,

TABLE III. Classification of order parameters. " ′ " indicates that the order is inter-orbital type. We use p to express p_y-wave orders, since p_x-wave orders do not appear.

(i, j)	Types of particle-hole order	Types of particle-particle order
$(0,0)$	Charge density wave (CDW)	d'-wave singlet SC(d'SS)
$(1,0)$	s'-wave charge density wave (s'CDW)	p_y-wave singlet SC (pSS)
$(2,0)$	p'_y-wave charge density wave (p'CDW)	s-wave singlet SC (sSS)
$(3,0)$	p_y-wave charge density wave (pCDW)	s'-wave singlet SC (s'SS)

$\phi_{\mu\nu}$ and $\theta_{\mu\nu}$, in the four sectors, $\mu = c, s$, and $\nu = 0, \pi$. In a fully gapped situation, in each sector, one of $\phi_{\mu\nu}$ or $\theta_{\mu\nu}$ is pinned at a value which may be 0 or $\pi/2$ (mod π); the conjugate variable fluctuates strongly. Naively this implies $(2 \times 2)^4 = 256$ possible insulating states, but only a few of these are relevant. The charge conservation implies that only ϕ_{c0} can be pinned, and the gauge invariance under translating all angles by $\pi/2$ allows us to set $\langle \phi_{c0} \rangle = 0$. The spin conservation means that only ϕ_{s0} can be pinned and additional constraints arising from the structure of the interactions may further limit the possibilities. In the end, only eight density-wave states and the corresponding eight dual Mott insulating states are relevant. The Mott states are obtained from the density-wave states by interchanging which of $\phi_{s\pi}$ and $\theta_{s\pi}$ is pinned. The pinned values of bosonic variables in the sixteen insulating phases are given in Table IV.

The density-wave states have a straightforward description in terms of local order parameters defined as

TABLE IV. Expectation values of bosonic variables in the fully gapped phases. We set $\langle \phi_{c0} \rangle = 0$. The commonly used names are given in parentheses. SP: spin-Peierls, SF: staggered flux, PDW: p-wave density wave, FDW: f-wave density wave.

Phase	$\langle \phi_{c\pi} \rangle$	$\langle \theta_{c\pi} \rangle$	$\langle \phi_{s0} \rangle$	$\langle \phi_{s\pi} \rangle$	$\langle \theta_{s\pi} \rangle$
CDW	$\pi/2$		$\pi/2$	$\pi/2$	
BDW(SP)	0		0	0	
s'CDW(CDW$_\pi$)		$\pi/2$	0		0
s'BDW(PDW)		0	$\pi/2$		$\pi/2$
p'CDW(SF)		0	0		0
p'BDW (FDW)		$\pi/2$	$\pi/2$		$\pi/2$
pCDW(ODW)	$\pi/2$		0	0	
pBDW(SP$_\pi$)	0		$\pi/2$	$\pi/2$	
HC	$\pi/2$		$\pi/2$		$\pi/2$
RS	0		0		0
S-Mott		$\pi/2$	0	0	
S'-Mott		0	$\pi/2$	$\pi/2$	
D-Mott		0	0	0	
D'-Mott		$\pi/2$	$\pi/2$	$\pi/2$	
HO	$\pi/2$		0	0	
RT	0		$\pi/2$		$\pi/2$

local combinations of fermion bilinears. The transcription is given in the previous section, and will not be elaborated on here with one proviso: the gap in the total charge mode implies a breaking of translational invariance, corresponding to a U(1) invariance in boson language. Therefore, only a $\mathcal{Z}_2$ invariance (shift of ϕ_{c0} by $\pi/2$) remains, and this allows us to distinguish site centered states (CDW's), and bond centered states (BDW's).

Dual to the density-wave stats are the Mott insulating states. These evolve into superconducting states upon doping. We do not know a general representation in terms of bilinears constructed from the original fermion operators, even if non-local string states are allowed. In some cases, approximate wave functions can be written down in the strong coupling limit, essentially by analogy to the superconducting states that appear upon doping:[10,16,22]

$$|S\text{-Mott}\rangle \equiv \prod_i \left[c^\dagger_{iA\uparrow} c^\dagger_{iA\downarrow} + c^\dagger_{iB\uparrow} c^\dagger_{iB\downarrow} \right] |0\rangle,$$

$$|D\text{-Mott}\rangle \equiv \prod_i \left[c^\dagger_{iA\uparrow} c^\dagger_{iA\downarrow} - c^\dagger_{iB\uparrow} c^\dagger_{iB\downarrow} \right] |0\rangle,$$

$$|RS\rangle \equiv \prod_i \left[c^\dagger_{iA\uparrow} c^\dagger_{iB\downarrow} - c^\dagger_{iA\downarrow} c^\dagger_{iB\uparrow} \right] |0\rangle,$$

$$|RT\rangle \equiv \frac{1}{2} \prod_i \left[c^\dagger_{iA\uparrow} c^\dagger_{i+1,B\downarrow} - c^\dagger_{iA\downarrow} c^\dagger_{i+1,B\uparrow} - (A \leftrightarrow B) \right] |0\rangle,$$

$$(31)$$

where RS stands for the rung-singlet state, and RT for the rung-triplet state.[14,34] These four states evolve into the sSS, pSS, s'SS, and d'SS states upon doping respectively. The bonding counterpart of these phases are the S'-Mott, D'-Mott, Haldane-charge (HC), and Haldane-orbital (HO) phases.[24] However, finding wave functions for these four Mott states remains a challenge.

Also, in some particular cases, string operators can be constructed. For example, in the strong-coupling limit, where the charge mode is decoupled, we expect the RS and RT states become the ones which appear in spin-$\frac{1}{2}$ Heisenberg two-leg ladders.[14,34] We note that the authors of Ref. 16 argued that the D-Mott, and S'-Mott states are adiabatically connected to the RS and RT states in the strong coupling limit. However, in the model studied here, the strong coupling limit of the D-Mott state has local singlet configurations which are different from those

of the RS state, and furthermore the S'-Mott state does not have a simple wave function in the real-space. The RS state appears in chains with antiferromagnetic coupling along rung (or ferromagnetic coupling over plaquette diagonals), and it is a resonance-valence-bond (RVB) state whose stable configurations are the singlet along rung or ladder. This state is characterized by a non-zero expectation value of a string operator

$$\langle\left(S^z_{A,i}+S^z_{B,i+1}\right)e^{i\pi\sum_{k=i+1}^{j-1}\left(S^z_{A,k}+S^z_{B,k+1}\right)}\left(S^z_{A,j}+S^z_{B,j+1}\right)\rangle,\tag{32}$$

and exhibits a "hidden antiferromagnetic order"; the total spin over plaquette diagonals, $S^z_{A,i}+S^z_{B,i+1}$, align antiferromagnetically along ladder except spin-0 site.

For chains coupled ferromagnetically along rung (or antiferromagnetically over plaquette diagonals), the above order disappears, and the RT state with the Valence-Bond-Solid (VBS) configuration[35] becomes stable. Singlet pairs are formed in a staggered manner, and this results in triplet pair along a rung. The following order parameter takes a non-vanishing value,

$$\langle\left(S^z_{A,i}+S^z_{B,i}\right)e^{i\pi\sum_{k=i+1}^{j-1}\left(S^z_{A,k}+S^z_{B,k}\right)}\left(S^z_{A,j}+S^z_{B,j}\right)\rangle,\tag{33}$$

which represents a hidden order about the spin-triplet on a rung.

The string operators for these disordered states are non-local, so complications arise in the transcription to bosonic variables. A generally accepted form for Eqs. (32) and (33) are:[36]

$$\langle\cos(\phi_{s0}(x))\cos(\phi_{s0}(y))\rangle,$$
$$\langle\sin(\phi_{s0}(x))\sin(\phi_{s0}(y))\rangle.\tag{34}$$

These correlation functions take non-zero values for the RS and RT phases respectively.

The bonding counterparts of the RS and RT phases are the Haldane-charge (HC), and Haldane-orbital (HO) phases proposed by Nonne et $al.$[24] as the Haldane gapped states of pseudo spin-1 antiferromagnetic Heisenberg chain; this realizes when the charge or orbital symmetry is promoted from U(1) to SU(2). The form of string operators for these states is similar to Eq. (33) if we replace the SU(2) spin operators by the charge and orbital SU(2) operators:

$$J^z_i=\frac{1}{2}(n_i-2),\ \ J^\dagger_i=c^\dagger_{i,A\uparrow}c^\dagger_{i,B\downarrow}-c^\dagger_{i,A\downarrow}c^\dagger_{i,B\uparrow};\tag{35}$$

$$T^z_i=\frac{1}{2}(n_{A,i}-n_{B,i}),\ \ T^\dagger_i=c^\dagger_{i,A\uparrow}c_{i,B\uparrow}+c^\dagger_{i,A\downarrow}c_{i,B\downarrow}.\tag{36}$$

The bosonized form of the strong operators are

$$\langle J^z_i e^{i\pi\sum_{k=i+1}^{j-1}J^z_k}J^z_j\rangle\sim\langle\sin(\phi_{c0}(x))\sin(\phi_{c0}(y))\rangle,$$
$$\langle T^z_i e^{i\pi\sum_{k=i+1}^{j-1}T^z_k}T^z_j\rangle\sim\langle\sin(\phi_{c\pi}(x))\sin(\phi_{c\pi}(y))\rangle,\tag{37}$$

where $\nabla\phi_{c0}\sim J^z(x)$ and $\nabla\phi_{c\pi}\sim T^z(x)$. These expressions become non-zero for the HC and HO phases respectively.

V. DUALITY, AND DYNAMICAL SYMMETRY ENLARGEMENT

A. Possible ground states

Two of the most prominent features of one-dimensional systems are $duality$[22–24] and $dynamical\ symmetry\ enlargement\ (DSE)$.[10,20] The idea of duality is based on the observation that the low energy theory is invariant under some discrete operations apart from the continuous symmetries listed in Table I. These discrete symmetries enable us to relate one ground state to another, and to understand quantum phase transitions among them.

DSE means that the effective theory describing the low energy fixed point exhibits a higher symmetry than that of the original lattice Hamiltonian. This phenomenon was noted by Lin et $al.$[10], who found that the low-energy theory of half-filled two-leg Hubbard ladder is the SO(8) Gross-Neveu (GN) model. Since their work, DSE has been seen in other multiband systems.[37,38] Combining these two ideas, we will identify the possible ground states for our models, taking DSE for granted.

Now, as a preparation, in order to exhibit the symmetries of the Hamiltonian, we refermionize the model using eight Majorana fermions as explained in Refs. 13, and 26. We decompose each mode into two Majorana fermions as

$$\psi^{c0}_r=\frac{1}{\sqrt 2}\left(\xi^7_r+i\xi^8_r\right),\ \ \psi^{c\pi}_r=\frac{1}{\sqrt 2}\left(\xi^5_r+i\xi^6_r\right),$$
$$\psi^{s0}_r=\frac{1}{\sqrt 2}\left(\xi^1_r+i\xi^2_r\right),\ \ \psi^{s\pi}_r=\frac{1}{\sqrt 2}\left(\xi^4_r+i\xi^3_r\right).\tag{38}$$

At half filling, the obtained expression for the U(1)$_o$ symmetric case, (a), is,

$$\begin{aligned}\mathcal{H}=&-i\frac{v}{2\pi}\sum_{a=1}^{8}(\xi^a_R\partial\xi^a_R-\xi^a_L\partial\xi^a_L)\\&+\frac{g_1}{2}\kappa_s^2+g_2\kappa_s\kappa_o+g_3\kappa_s\kappa_I\\&+g_4\kappa_o\kappa_I+\frac{g_5}{2}\kappa_o^2+\frac{g_6}{2}\kappa_c^2\\&+g_7\kappa_s\kappa_c+g_8\kappa_o\kappa_c+g_9\kappa_I\kappa_c\end{aligned}\tag{39}$$

with $\kappa_s=\sum_{a=1}^{3}\xi^a_R\xi^a_L$, $\kappa_o=\sum_{a=4}^{5}\xi^a_R\xi^a_L$, $\kappa_I=\xi^6_R\xi^6_L$, and $\kappa_c=\sum_{a=7}^{8}\xi^a_R\xi^a_L$. The indices "$s$", "$o$", "$I$", and "$c$" refer to the SU(2)$_s$, U(1)$_o$, $\mathcal{Z}_2$, and U(1)$_c$ symmetries respectively.

Away from half filling, case (b), the charge mode is decoupled from the other modes, and we do not need to consider $g_{i=6\sim9}$. Thus, we have

$$\begin{aligned}\mathcal{H}=&-i\frac{v}{2\pi}\sum_{a=1}^{6}(\xi^a_R\partial\xi^a_R-\xi^a_L\partial\xi^a_L)\\&+\frac{g_1}{2}\kappa_s^2+g_2\kappa_s\kappa_o+g_3\kappa_s\kappa_I\\&+g_4\kappa_o\kappa_I+\frac{g_5}{2}\kappa_o^2.\end{aligned}\tag{40}$$

TABLE V. Possible ground states for case (a)–(d) in Table I at equal velocities. The BDW, CDW, S-Mott, and sSS phases in the second column are expressed by the fundamental SO(8) or SO(6) Gross-Neveu model for case (a)–(d) respectively. The other states are mapped from these fundamental states by the duality transformation Ω in the top row. Ω_ν is an operation of $\xi_L^a \to -\xi_L^a$ for all the a's in a symmetry sector ν. For example, in case (a), the BDW state is mapped to the p'CDW state by Ω_o. For doped cases, (b) and (d), the charge mode is separated from the rest, and the ground states are invariant under Ω_c.

	1	Ω_c	Ω_o	$\Omega_{c,o}$	Ω_I	$\Omega_{c,I}$	Ω_s	$\Omega_{c,s}$
(a)	BDW	CDW	p'CDW	p'BDW	S-Mott	S'-Mott	RT	HO
(b)	CDW	CDW	p'CDW	p'CDW	sSS	sSS	d'SS	d'SS
(c)	S-Mott	S'-Mott	D-Mott	D'-Mott	s'CDW	s'BDW	p'BDW	p'CDW
(d)	sSS	sSS	pSS	pSS	s'CDW	s'CDW	p'CDW	p'CDW

As we mentioned before, even without an explicit U(1) orbital symmetry for the lattice Hamiltonian, the low energy theory may have the effective $\widetilde{U(1)}_o$ symmetry.[10,21,24] In that case, the structure of the refermionized forms are the same as above. Thus, cases (c) and (d) have the same form as Eqs. (39) and (40) with different values of g's.[Note1]

For the refermionized forms, duality mappings are defined as, $\xi_L^a \to -\xi_L^a$ while keeping right-moving parts untouched. It is easy to see that Eqs. (39) and (40) are invariant under such transformations if we change the signs of some coupling constants as well. To retain the form of the Hamiltonian, only mappings that transform all the Majorana fields in the same symmetry sector are permitted. For example, for the SU(2) spin part, we should map the three left Majorana fermions, $\xi_L^{a=1\sim3}$, at the same time. For notational convenience, we define Ω_ν as an operation of $\xi_L^a \to -\xi_L^a$ for all the a's in a symmetry sector ν. With this at hand, it is obvious that allowed mappings for half filling cases are

$$\Omega_{O(8)} \equiv \{\Omega_c, \Omega_o, \Omega_I, \Omega_s, \Omega_{c,o}, \Omega_{c,I}, \Omega_{o,I}\}. \quad (41)$$

The number of independent mappings is three, and other mappings just follow from them ,e.g., $\Omega_{o,I} = \Omega_o\Omega_I$. Away from half filling, the charge mode is separated, so only three of the above mappings are left,

$$\Omega_{O(6)} \equiv \{\Omega_o, \Omega_I, \Omega_s\}, \quad (42)$$

and two of them are independent. An immediate consequence of these dualities and DSE is that although we showed sixteen insulating phases for half filling systems, and eight metallic phases for incommensurate filling, only a part of them are realized.

Now, we will show such possible ground states for each model. We start from the "fundamental" SO(8) Gross-Neveu (GN) model,

$$\mathcal{H} = -i\frac{v}{2\pi}\left(\vec{\xi}_R\partial\vec{\xi}_R - \vec{\xi}_L\partial\vec{\xi}_L\right) + \frac{g}{2}\left(\vec{\xi}_R\vec{\xi}_L\right)^2, \quad (43)$$

which appears at low-energy when all the g's in Eq. (39) converge to the same value as a result of DSE. For case (a), this model represents the BDW phase, and other possible phases are found by applying $\Omega_{O(8)}$ to the BDW state (see Table V). We denote them as Γ_y, and they are

$$\Gamma_y : \text{BDW, CDW, } p'\text{CDW, } p'\text{BDW,}$$
$$S\text{-Mott, } S'\text{-Mott, RT, HO.} \quad (44)$$

The case (b) follows from the relation between insulating states and metallic states, or applying $\Omega_{O(6)}$ to the CDW phase, which is "fundamental". The original lattice model we are considering here is invariant under the orbital U(1) rotation about y-axis. As we mentioned in Sec. III, the generator of this symmetry cannot be expressed by a single local bosonic field within Abelian-bosonization scheme.

This combination, Γ_y, is different from the ones which have been studied extensively; previously studied phases are

$$\Gamma_z : \text{BDW, CDW, } p\text{BDW, } p\text{CDW, RS, HC, RT, HO} \quad (45)$$

and

$$\widetilde{\Gamma_z} : S\text{-Mott, } S'\text{-Mott, } D\text{-Mott, } D'\text{-Mott,}$$
$$s'\text{CDW, } s'\text{BDW, } p'\text{BDW, } p'\text{CDW.} \quad (46)$$

The former, Γ_z, appears in models with weak transverse hopping, and with the U(1)$_o$ symmetry about z-axis.[24,30] The latter, $\widetilde{\Gamma_z}$, appears when the model has strong transverse hopping, and the low energy theory possesses the $\widetilde{U(1)}_o$ symmetry;[7,10,12,16,17] our cases (c) and (d) belong to this category (see Table V).

The connection between Γ_y and Γ_z is obvious. Since the generator of the orbital symmetry for each case is y- or z-component of Eq. (36), they are simply mapped to each other by a rotation around x-axis:

$$R_x : \begin{pmatrix} c'_{rAs} \\ c'_{rBs} \end{pmatrix} = \frac{1}{\sqrt{2}}\begin{pmatrix} 1 & -i \\ -i & 1 \end{pmatrix}\begin{pmatrix} c_{rAs} \\ c_{rBs} \end{pmatrix}. \quad (47)$$

This transformation does not affect the charge and spin generators. For instance, the S'-Mott state in Γ_y goes to the HC state in Γ_z by R_x. The correspondence among other states is given in Fig. 2. On the other hand, $\widetilde{\Gamma_z}$ and
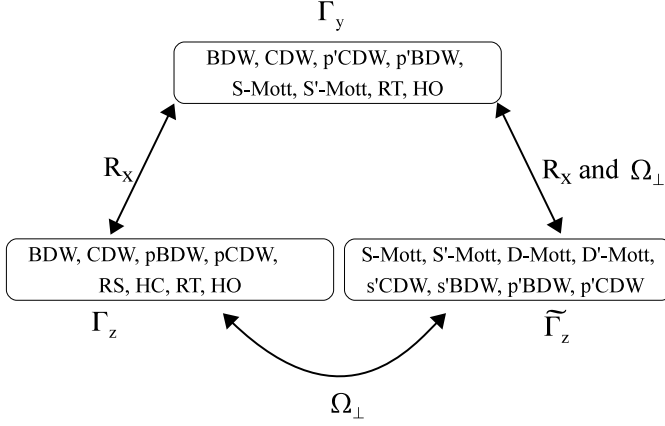
FIG. 2. Relationships among three groups of insulating ground states. R_x indicates the rotation about x-axis in orbital space in Eq. (47), and $\Omega_\perp$ is strong-weak tunneling duality mapping in Eq. (48). For example, the S'-Mott state in Γ_y maps to the HC state in Γ_z by R_x.

Γ_z transform each other by so-called *strong-weak tunneling duality*,[21,24]

$$\Omega_\perp: \quad c_{Lm\uparrow} \to c_{Lm\downarrow}^\dagger, \quad c_{Lm\downarrow} \to -c_{Lm\uparrow}^\dagger. \qquad (48)$$

Therefore, we found that in addition to underlying band structure, the form of interaction also affects the possible combinations of ground states. We summarized these results in Table V and Fig. 2.

B. Quantum phase transition

The quantum phase transitions among gapped ground states could be either first order or second order. For the transitions among states connected by a duality mapping, the modes which are not involved in the mapping become massive at higher energy, and the effective low energy theory near the transition contains only Majorana fields flipped by the mapping.[23]

For a single Majorana field, it becomes the critical Ising model,

$$\mathcal{H} = -i\frac{v}{2\pi}\left(\xi_R\partial\xi_R - \xi_L\partial\xi_L\right) - im\xi_R\xi_L \qquad (49)$$

Over the transition, the mass changes its sign, and this represents a second-order phase transition. With more than one field, the low-energy effective theory becomes the massive O(N) Gross-Neveu (GN) model,

$$\mathcal{H} = -i\frac{v}{2\pi}\left(\vec{\xi}_R\partial\vec{\xi}_R - \vec{\xi}_L\partial\vec{\xi}_L\right) - im\vec{\xi}_R\vec{\xi}_L + \frac{g}{2}\left(\vec{\xi}_R\vec{\xi}_L\right)^2. \qquad (50)$$

The fate of further renormalization to lower energy determines whether the phase transition is first-order or second-order depending on the final fixed point for the

critical fields.[10,16,21,40,41] The transition line is defined as the point where the m in Eq. (50) goes to zero, and the critical fields are expressed by a massless GN model in the vicinity of transition. For $N = 2$, it is known that the system can be mapped to a Gaussian model, so it is a second order transition. For $N \geq 3$, however, if the coupling constant in the GN model is positive ($g > 0$), the renormalization flow departs to a strong coupling fixed point (asymptotic free), since RG equation is given by

$$\dot{g} \propto g^2. \qquad (51)$$

At this fixed point, the mass is generated dynamically, and the system is off-critical. We can see this either by mean-field treatment of the interaction (reducing the quartic part to quadratic with the order parameter $\langle\xi_R\xi_L\rangle$), or by stationary phase approximation, which becomes exact when $N \to \infty$. At this massive fixed point, there are two degenerate minima about two signs of mass, and they correspond to two phases connected by this first-order transition. On the other hand, when $g < 0$, further renormalization reduces g to 0, and the system reaches a massless fixed point; this represents a second-order transition.

When the transition is second order, the critical theory is described by a conformal field theory (CFT) due to its dimensionality, (1+1). Each CFT is characterized by its central charge, c, which roughly expresses the number of critical fields. $c = 1/2$ is the $\mathcal{Z}_2$ Ising critical theory, $c = 1$ is the U(1) Gaussian theory, and $c = 3/2$ is the SU(2)$_2$ Wess-Zumino-Novikov-Witten theory. With the duality mappings, it is easy to read off the central charge of each CFT. Since each Majorana fermion carries $c = 1/2$, the number of fields flipped by a mapping directly tells us the central charge. We will identify the phase transitions appearing in our phase diagrams more precisely in the next section.

VI. RG EQUATIONS AND PHASE DIAGRAMS

In the RG equations obtained from Abelian bosonization, we use normalized coupling constants defined as

$$y_i \equiv \frac{g_i}{4\pi v}. \qquad (52)$$

RG equations are derived using the operator product expansion (OPE)[7,42,43] and integrating out higher frequency modes. The RG equations are complicated, so we will not show them explicitly. In all of the cases which we have examined, the RG equations may be expressed as

$$\frac{dy_i}{dl} = -\frac{\partial V}{\partial y_i}. \qquad (53)$$

with a potential function, $V[y_1(l), y_2(l), \cdots, y_n(l)]$. The RG flow is to the valleys of the potential in the beginning and then along the valley. The potential structure

is consistent with the arguments of Ref. 44, which suggests that the presence of a potential function is related

to Zamolodchikov's c-theorem.[45] For the commensurate case, $k_A = k_B = \pi/2$, the potential is

$$
\begin{aligned}
V[y_i] = & -y_{1a}y_{1c}y_{\|c} + y_{1a}y_{1b}y_{2a} - y_{1a}y_{3a}y_{\|b} + y_{1c}y_{1d}y_{2c} - y_{1c}y_{3c}y_{\|b} + y_{1d}y_{\|a}y_{1b} \\
& + y_{1d}y_{3b}y_{\|b} - y_{2c}y_{3b}y_{3c} - y_{\|c}y_{3a}y_{3c} + y_{1b}y_{3d}y_{\|b} - y_{2a}y_{3a}y_{3d} + y_{\|a}y_{3b}y_{3d} \\
& - \frac{1}{2}\left(y_{3a}^2 - y_{3b}^2 - y_{3c}^2 - y_{3d}^2 - y_{\|b}^2 \right) y_{c0} - \frac{1}{2}\left(-y_{1c}^2 - y_{2c}^2 - y_{\|c}^2 + y_{\|a}^2 + y_{1b}^2 + y_{2a}^2 - y_{3c}^2 + y_{3d}^2 \right) y_{c\pi} \\
& - \frac{1}{2}\left(y_{1d}^2 + y_{1a}^2 + y_{1c}^2 + y_{1b}^2 + y_{\|b}^2 \right) y_{s0} - \frac{1}{2}\left(y_{1d}^2 - y_{1a}^2 + y_{2c}^2 - y_{\|c}^2 + y_{\|a}^2 - y_{2a}^2 - y_{3a}^2 + y_{3b}^2 \right) y_{s\pi},
\end{aligned}
\tag{54}
$$

where we introduced $K_{\mu\nu} \equiv 1 - y_{\mu\nu}$ for each Luttinger parameter. For $k_A \neq k_B$ or doped cases, we should remove some coupling constants which are not allowed by momentum conservation. The RG equations valid even when velocities are different are given in Appendix B. We checked that both RG equations give consistent results when $v_A = v_B$.

To get phase diagrams, we integrated the RG equations numerically until one of the coupling constant becomes of the order of $1(\equiv t)$. We used initial values of coupling constants as small as 10^{-8}–10^{-3}. Due to the hidden potential structure, the asymptotic behavior of the RG flow is captured by the following ansatz,[7,44]

$$
g_i'[l] = \frac{g_{0i}}{l_c - l}, \tag{55}
$$

where l_c is the length at which the relevant couplings diverge, and the g_{0i} determines the ratio among them. This represents the fixed ray of relevant coupling constants. Then, the bosonic fields are pinned down to the minima of the effective potential. These values enable us to determine the order parameter which takes a non-zero value.

The obtained phase diagrams are shown in Figs. 3–7. They correspond to the various cases in Table I. We also investigated the effect of velocity anisotropy to the phases in physically relevant parameter region, $0 < J < U/2$, using the RG equations based on the fermionic Hamiltonian. We studied the range, $1 \leq v_A/v_B \leq 10$.

At various points in the following discussion, we also label the phases in the "$CnSm$" notation, which indicates n massless charge modes and m massless spin modes introduced in Ref. 7.

A. $k_A = k_B = \pi/2$ at half filling

First, we look at case (a), where $k_A = k_B$ at half filling (Fig. 3). Absence of the HO phase indicates that the system does not flow to the enlarged orbital SU(2) symmetry state, although this could happen in principle by changing initial conditions. The RT phase, a high spin sate, resides in $0 < J < U$ region, which may be accessible in real material.
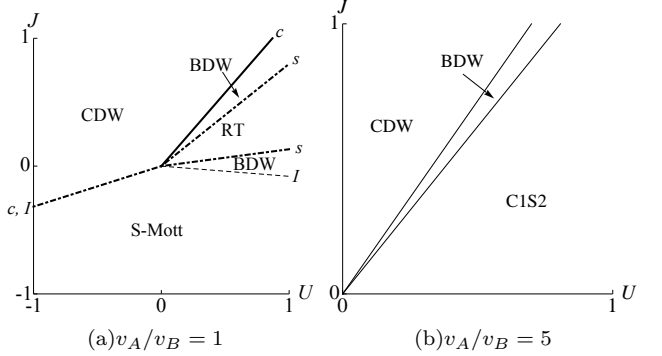

FIG. 3. Phase diagram for case (a), $k_A = k_B = \pi/2$ with equal velocities. Physically relevant region is $0 < J < U/2$. A dashed line indicates SU(2) or first order transition. A solid line is a Gaussian theory, and a dotted line is an Ising transition. "c", "o", "s", and "I" indicate the critical fields on the transition line. All of these phases are $C0S0$.

Although precise boundaries do not coincide exactly, the corresponding Hartree-Fock (HF) phase diagram shows similar structure.[29] There we have the SDW phase instead of the RT state in $0 < J < U$; they are both locally high-spin configurations with anti-ferromagnetic orders along the chain. The S-Mott state found in the bosonization result corresponds to mainly the degenerate state of the s'CDW and pCDW orders with a smaller region of sSS in the HF phase diagram. In the bosonic language, the order parameter of the sSS phase is the same as that of the S-Mott state except the total charge mode. The s'CDW and pCDW states are degenerate due to the orbital symmetry, and they are Ising dual to the S-Mott and Haldane orbital (HO) phases respectively. The HO phase does not appear in the bosonic calculation, but it is connected to the S-Mott phase by the duality mapping of the orbital sector (see Table V). The CDW state stays almost the same regime in both phase diagrams. The BDW phase does not appear in the HF phase diagrams, since its HF energy is higher than that of the CDW phase.

The critical properties of the CDW-BDW transition are given by a U(1) Gaussian theory of the charge sec-

tor, while those of the BDW-S-Mott transition are given by the $\mathcal{Z}_2$ Ising theory. The rest of transitions are either SU(2) criticality or first order; the critical fields at the BDW-RT transition line are spin modes, and at the CDW-S-Mott line are the charge and Ising fields.

We noticed that the phase transition from the RT state to the CDW state with increasing J is similar to the SDW-CDW transition found in the extended Hubbard model (EHM).[46,47] The EHM has a nearest neighbor interaction, Vn_jn_{j+1}, in addition to the Hubbard interaction, $Un_{j\uparrow}n_{j,\downarrow}$. As the former interaction becomes predominant, particles try to form a CDW state, while strong U prefers SDW. In the weak coupling regime, it is found that the SDW state undergoes a spin-gap transition to a BDW state, and then becomes the CDW state through a Gaussian transition of the charge sector. In the strong-coupling regime, these two transition lines are coupled to a first order transition line. In our model, strong J plays the same role as V in the EHM; large J induces an attractive on-site interaction [see Eq. (2)] leading to the CDW state. The properties of transitions from the RT phase to the CDW phase, and the existence of the narrow BDW region are also the same as in the EHM. Therefore, we expect that in the strong-coupling regime, the RT-CDW transition in our model also becomes first order, although this has not been demonstrated.

Now, we consider the effect of velocity difference in the first quadrant; $U, J > 0$ [Fig. 3(b)]. As v_A/v_B becomes as large as 1.5, we found that the RT and BDW states in small $J > 0$ are completely replaced by a $C1S2$ state, where only a charge mode of a single band becomes massive, and the rest is massless. The CDW and BDW states in $J > U > 0$ are robust to the change in velocity. This is because the large anisotropic velocities suppress the interband scattering, resulting in the domination of intraband scattering. As v_A/v_B is increased beyond 1.5, the $C1S2$ phase becomes larger, although the BDW phase always exists between the CDW and $C1S2$ phases.

B. $k_A = k_B$ at incommensurate filling

The phase diagram for $k_A = k_B$ with incommensurate filling is given in Fig. 4. This is similar to the one at half filling if we replace the insulating states to corresponding metallic ones; S-Mott to sSS, RT to d'SS, and BDW to CDW. The BDW sate near $J \simeq 0$ in Fig. 3 disappears. The transition between the CDW and d'SS states is governed by spin modes leading to the SU(2) criticality or first order transition. The CDW-sSS transition is an Ising transition, $c = 1/2$. Finally the d'SS-sSS transition is described by a Gaussian theory of the orbital sector.

The velocity difference in a quadrant, $U, J > 0$, does not modify the large J regime, though a $C2S1$ state appears at small J [Fig. 4(b)]. The $C2S1$ phase was observed in other two-leg ladder systems when the velocity difference becomes large.[7,12]
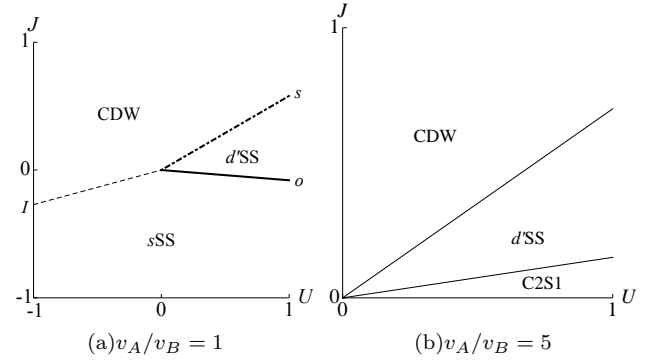
The HF phase diagram of this case[29] has the SDW

FIG. 4. Phase diagram for case (b), $k_A = k_B$ away from half filling with equal velocities. Physically relevant region is $0 < J < U/2$. A dashed line indicates SU(2) or first order transition. A solid line is a U(1) Gaussian theory, and a dotted line is an Ising transition. "c", "o", "s", and "I" indicate the critical fields on the transition line. All of these phases are $C1S0$.

phase for $0 < J < 0.6U$, which corresponds to the d'SS phase found by bosonization; both of them are locally high-spin states. In the negative J region, we have the sSS state in Fig. 4, while the HF calculation gives not only the sSS state, but also a large region of the s'CDW phase. As we mentioned, this CDW state is Ising dual to the S-Mott phase, which is the insulating analogue of the sSS state. In the large $J > 0$ region, we found p'_y-wave spin-triplet superconductivity in the HF phase diagram, which is replaced by CDW in the bosonic calculation. The CDW state around $0 < J < -U$ is robust, and we observe it both at HF level and after renormalization.
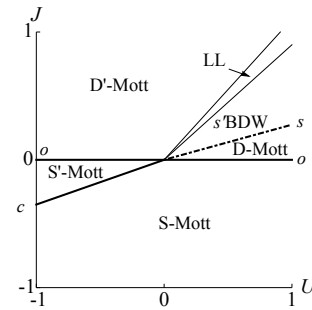
C. $k_A \neq k_B$ at half filling

FIG. 5. Phase diagram for case (c), $k_A \neq k_B$ at half filling with equal velocities. Physically relevant region is $0 < J < U/2$. A dashed line indicates SU(2) or first order transition. A solid line is a U(1) Gaussian theory. A thin line indicates KT transition. "c", "o", "s", and "I" indicate the critical fields on the transition line.

For the system at half filling, but with two different Fermi momenta, the phase diagram is given in Fig.

5. There is a narrow Luttinger Liquid (LL) phase near $U \simeq J > 0$, where all the modes are massless. The transition between massive phases and a LL phase is Kosterlitz-Thouless (KT) in the sense that a LL phase is critical and has power-low correlation, while massive phases have exponentially decaying correlations. The transitions among Mott phases all have a Gaussian criticality; the S-Mott-S'-Mott transition is governed by the charge sector, and others are by the orbital sector. On the other hand, the s'BDW-D-Mott transition line is the SU(2) criticality or first order. In this case, the velocity difference does not modify the phase diagram in physically relevant region essentially.

The corresponding HF phase diagram shows the SDW and s'SDW states in the physically relevant region,[29] while they are replaced by the s'BDW and D-Mott phases in the RG phase diagram. This is a notable difference between the result of two equivalent bands and that of inequivalent bands. For the $k_A = k_B$ cases, locally high-spin states, RT and d'SS, are dominant in $0 < J < U/2$, while low-spin configurations, s'BDW and D-Mott, are found in the $k_A \neq k_B$ case. We understand these low-spin states as a result of decoherence by two different wave numbers. In essence, density waves with different phases in the two bands mean that the energy contribution from the J interaction averages out to zero. The CDW phase, which dominates large positive J region at mean-field level, is replaced by the D'-Mott state after renormalization. For this case, the pSS state, the metallic analogue of the D'-Mott state, is subdominant with large positive J at the HF level, and this is more enhanced than the CDW order during the renormalization flow. Negative J region of the HF phase diagram is again covered by the sSS and s'CDW phases, which are related to the $S(')$-Mott state.

D. $k_A \neq k_B$ at incommensurate filling

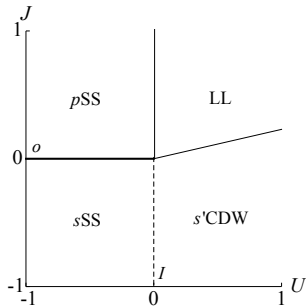

FIG. 6. Phase diagram for case (d), $k_A \neq k_B$ away half filling with equal velocities. Physically relevant region is $0 < J < U/2$. A solid line is a U(1) Gaussian theory, and a dotted line is an Ising transition. A thin line is KT transition. "c", "o", "s", and "I" indicate the critical fields on the transition line.

With inequivalent Fermi momenta and incommensurate filling (Fig. 6), the physically relevant region is covered by a LL phase, and the s'CDW phase. The pSS and sSS phases can be understood as the reminiscent of the D'-Mott and $S(')$-Mott states which exist at half filling. Again, transitions between the LL phase and massive phases are KT type except the total charge mode remaining massless in both phases. The phase transition between the pSS and sSS states is governed by a U(1) Gaussian criticality of the orbital sector. The transition between the s'CDW and sSS phases is Ising type. As the velocity anisotropy becomes larger, the s'CDW phase is gradually suppressed, and whole area in physically relevant region is covered by the LL state for $v_A/v_B \geq 6$.

The HF phase diagram in this case is similar to the RG phase diagram. We have the $p(s)$SS state with large negative U and small positive (negative) J. For large negative J, we have the s'CDW state. The pTS and SDW states appearing in positive J regime of the HF phase diagram are renormalized to the Luttinger liquid phase.

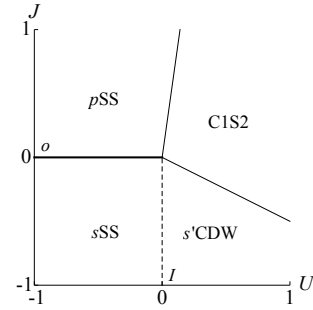### E. $k_A = \pi/2 \neq k_B$ at incommensurate filling

FIG. 7. Phase diagram for case (e), $k_A = \pi/2 \neq k_B$ away from half filling with equal velocities. Physically relevant region is $0 < J < U/2$. A solid line is a U(1) Gaussian theory, and a dotted line is an Ising transition. A thin line is KT transition. "c", "o", "s", and "I" indicate the critical fields on the transition line.

The phase diagram for the case with $k_A = \pi/2 \neq k_B$ (Fig. 7) is almost similar to that of case (d) except Luttinger liquid state is replaced by a $C1S2$ phase, where a commensurate band opens a charge gap, and the rest of the modes remain massless. This is an orbital-selective Mott state. The velocity anisotropy in both directions, $v_A/v_B < 1$ and $v_A/v_B > 1$, does not modify the $C1S2$ state in the region, $0 < J < U/2$. The HF phase diagram for this case is almost the same as the previous case with $k_A \neq k_B$ at incommensurate filling.

VII.   FULLY SPIN-POLARIZED CASE: CHARGE-ORBITAL MODEL

So far, we have limited our focus to the weak coupling limit. However, in multiorbital systems the strong-

coupling limit can bring qualitatively new effects.[29,48–51] In particular, in the physical ($J > 0$) case, one may expect every ion to be in the state of maximal spin consistent with given total occupation. In this circumstance, we expect antiferromagnetic order in the half-filled case, and when the system is slightly doped, more complicated structures such as phase separation and spiral phases will appear. At filling further away from $n = 2$, the system shows ferromagnetism (FM) with an orbital order. Considering the fact that ferromagnetic states dominate the phase diagram at most fillings,[29,51] in this section, we investigate the possible orbital orders assuming that the system is fully spin polarized. In other words, we consider the effect of residual backscattering in the subspace of the charge and orbital sectors assuming the spin excitations are frozen. We leave the investigation of the regime close to half filling for future study.

Suppose that all the electrons have the same spins, the model in Eq. (1) and Eq. (2) is then reduced to,

$$H = H_{\text{kinetic}} + \sum_i (U - 3J)\, n_{iA} n_{iB}, \qquad (56)$$

where we omit the spin index. Now the $SU(2)_s$ symmetry is lost, but we can regard the orbital part as pseudo spins. If the two bands have the same k_F and velocities, the system has the orbital $SU(2)$ symmetry. The band splitting in orbital sector is isomorphic to the Zeeman splitting by magnetic field. Therefore, the model now turns to a simple Hubbard model with effective interaction $U_{\text{eff}} = U - 3J$, with or without magnetic field.

Depending on the effective crystal field splitting between the two orbitals Δ, and the band widths, there may be three different scenarios in this model. The first case is that the two bands are completely degenerate: $\Delta = 0$, and $k_A = k_B$. We expect a staggered orbital order to appear. On the other hand, when there exists either small splitting or when the band widths are slightly different, the two momenta are not equal, and orbital orders might be suppressed. We will discuss these two scenarios below using bosonization method. However, there is another scenario, which may arise when either splitting is large, or two band widths are greatly different. Then, only one band has states at the Fermi surface and the physics is trivial.

We first look at the degenerate case, $k_A = k_B$, corresponding to the absence of magnetic field. The bosonized form of the Hamiltonian in Eq. (56) at half filling is given by

$$
\mathcal{H} = \frac{1}{2\pi} \sum_{\nu=c,o} v_\nu \left[K_\nu (\nabla \theta_\nu)^2 + \frac{1}{K_\nu} (\nabla \phi_\nu)^2 \right] \\
+ \frac{2}{(2\pi\alpha)^2} U_{\text{eff}} \cos\left(2\sqrt{2}\phi_o\right) \qquad (57) \\
- \frac{2}{(2\pi\alpha)^2} U_{\text{eff}} \cos\left(2\sqrt{2}\phi_c\right),
$$

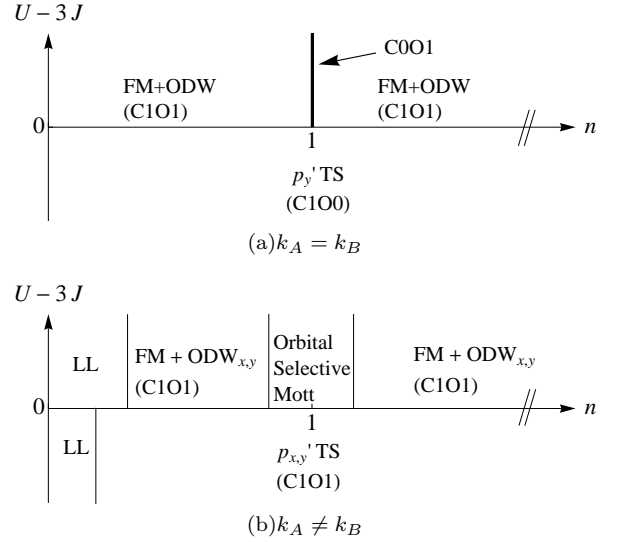FIG. 8. Schematic phase diagrams for the spin-polarized model for two equivalent bands or slightly different bands. When $k_A \neq k_B$, the ODW_x and ODW_y phases have the same correlation exponent, and so do p'_xTS and p'_yTS. Filling closer to $n = 2$ is not investigated. "$CnOm$" represents a state with n massless charge modes and m massless orbital modes.

where the Luttinger parameters and velocities are,

$$K_c v_c = K_o v_o = v \qquad (58)$$

$$v_{c(o)}/K_{c(o)} = v\left(1 \pm \frac{U_{\text{eff}}}{\pi v}\right). \qquad (59)$$

Thus, the charge and orbital modes are decoupled, and each mode has a $SU(2)$ symmetry. The total symmetry is $SU(2) \times SU(2) = SO(4)$.

Translating the analysis for the Hubbard model[32] to our charge-orbital model, we found the following results. For incommensurate filling, the last Umklapp term in Eq. (57) vanishes, and the charge mode is massless. Also the $SU(2)_c$ symmetry is broken to $U(1)_c$. About the orbital sector, we find:

(1) $U_{\text{eff}} > 0$: Orbital density wave (ODW) has the longest correlation, and both orbital and charge modes are massless. The $SU(2)_o$ symmetry requires that ODW's about all three directions (x, y, z) are degenerate.

(2) $U_{\text{eff}} < 0$: The orbital sector becomes massive, and the phase with slowest decaying correlation is orbital-singlet superconductivity with parallel spins, i.e., p'_yTS in Ref. 29.

At half filling, the charge mode becomes massive ($K_c = 1/2$) when the effective interaction is repulsive; the system is Mott insulating. The orbital part still gives ODW, and this FM+ODW state in $U > 3J$ regime is observed both analytically[29,48,49] and numerically.[50,51] For the attractive side, the charge mode is gapless ($K_c = 1$) with

an orbital gap by the p'_yTS order; this is the Luther-Emery phase. This triplet superconductivity agrees with the numerical result by Sakamoto *et al.*.[51] The results are summarized in Fig. 8(a).

Now we turn to the case with $k_A \neq k_B$; there is a pseudo magnetic field acting on the orbital space. At very small filling, only a single band is filled, so the ground state is ferromagnetic Luttinger liquid of a single gapless mode. When we dope enough the two bands start to share the Fermi surface. The $SU(2)_o$ symmetry is reduced to $U(1)_o$, and the $\cos\left(2\sqrt{2}\phi_o\right)$ term vanishes due to two different Fermi momenta. Thus, the orbital sector is always massless. With an attractive interaction, the band degeneracy occurs with smaller filling than with a repulsive interaction, since we guess the upper band is pulled down by the lower filled band for $U_{\text{eff}} < 0$. The charge mode is massive (massless) for repulsive (attractive) interaction at half filling. At tree-level, the states with longest correlations are ODW_x and ODW_y for $U_{\text{eff}} > 0$, and p'_xTS and p'_yTS for $U_{\text{eff}} < 0$. Since the orbital symmetry is explicitly broken, the exponents of correlation may differ for different directions. Finally, contrary to the complete degenerate case, we speculate that an orbital selective Mott phase appears near $n = 1$ for inequivalent bands; once one band is half filled, the commensurate wave vector opens a gap, and the other band remains metallic. Further filling just goes to the metallic band until it reaches half filling. Fig. 8(b) presents the general phase diagram for this case.

VIII. CONCLUSION

In this paper, we investigated a two-orbital Hubbard model which may encapsulate phenomena realized in transition-metal nanowires. Along with many aspects of two-leg ladder models, unique properties of transition-metal d-orbitals lead to several new results.

In our analysis, we used the ideas of dynamical symmetry enlargement[10,20,21] and duality relations[23,24] to list eight insulating phases at half filling, and six metallic phases away from half filling. Each phase is represented by a Gross-Neveu model at low energy, and phases are related to each other by duality mappings. The same analysis was done for weak-tunneling models with the $U(1)_o$ symmetry about z-axis,[24,30] and for strong-tunneling models with the $\widetilde{U(1)}_o$ symmetry.[10,16,17]. Some cases we studied in this paper belong to the latter category, and we obtained the same results. However, we also studied a model with a different orbital symmetry, the $U(1)_o$ symmetry about y-axis, and found that this form of interaction gives rise to a new combination of ground states; half of which were found in weak-tunneling systems and the other half were in strong tunneling systems. This is because the underlying orbital rotational symmetry involves a generator which cannot be written by a single local bosonic field. The quantum phase transitions among those ground states were also briefly sum-

marized using Gross-Neveu models as low-energy effective theories.[16,23] The new combinations of ground states we found means that the model we proposed can exhibit new kinds of quantum phase transitions.

After classifying the possible ground states, we determined the ground state of the model by numerically integrating the RG equations. The phase diagrams are presented in Figs. 3–7. The essential results for physically relevant regime, $0 < J < U/2$, are as follows:

(1): For two equivalent bands at half filling, we found a high spin state, RT, for relatively large J, and a low spin state, BDW, for small J (Fig. 3). Keeping $k_A = k_B$ but introducing a velocity difference causes these phases to be replaced by a $C1S2$ state where only a charge mode in a single band becomes massive. Upon doping, the RT state turns into the d'SS state and the BDW state disappears (Fig. 4). A velocity difference leads to a $C2S1$ phase for small J, but the d'SS state still survives in large J.

(2): For the cases with two different Fermi momenta, similar RG analyses have been done.[7,8,16,17] Our main contribution for this case is that we identify the ground states for our specific model and interactions. The ground state in the physically relevant region is the s'BDW state for large J and the D-Mott state for small J at half filling (Fig. 5). These phases are robust to velocity differences. The surprising result here is that we have locally low-spin configurations even when $J > 0$, while completely degenerate bands give high-spin states, RT and d'SS, in the same parameter regime. We think the low-spin configurations are achieved by the destructive interference between two different Fermi momenta, and therefore, the complete orbital degeneracy is crucial to have locally high-spin states. When the system is away from half filling, a Luttinger liquid phase becomes dominant, although we observed the s'CDW phase for very small J (Fig. 6). This density wave state is wiped away by velocity difference, and replaced by the Luttinger liquid state. When only a single band is commensurate, the system exhibits an orbital-selective charge-gapped state due to the intraband Umklapp process while all the other modes remain massless (Fig. 7).

We also investigated the charge-orbital model obtained as a result of full spin-polarization. The model can be mapped to a Hubbard model with an effective interaction $U_{\text{eff}} = U - 3J$. For repulsive side, we find the FM+ODW phase with massless charge and orbital modes is stable at most of the fillings. When two bands are equivalent, we have a charge gap at $n = 1$, while we expect an orbital selective Mott phase around $n = 1$ for inequivalent bands. The attractive side is dominated by orbital singlet superconductivity with an orbital gap when two bands are equal. On the other hand, for inequivalent

bands, orbital singlet and triplet superconductivity have the longest correlation and the orbital gap is absent. The charge gap does not develop in the attractive side.

Finally we refer to possible experimental consequences. From the band calculation, it is plausible that the real Co nanowires exhibit a ferromagnetic state, meaning that the system has relatively strong correlations.[52] In particular, since U is much larger than J in real materials, we guess the best possible ground state is a ferromagnetic orbital density wave from the discussion in Section VII. Of course, we have to note that the result is based on strong assumptions such that the system is fully spin polarized, and that the number of the bands is just two.

Appendix A: Abelian Bosonization

In this appendix, we briefly recall formulas from Abelian-bosonization which are needed in the text.[31–33,53] The following formula gives transformation from a fermionic Hamiltonian to a bosonic Hamiltonian

$$\psi_{m\sigma r} = \frac{\eta_{m\sigma}}{\sqrt{2\pi\alpha}} e^{\mp i\Phi_{m\sigma r}} \quad (A1)$$

where $m = A, B$ is orbital, and $r = R, L$ is chirality. The bosonic fields satisfy the commutation relations,

$$[\Phi_{m\sigma R(L)}(x), \Phi_{m'\sigma' R(L)}(x')] = \pm i\pi\delta_{mm'}\delta_{\sigma\sigma'}\mathrm{sgn}(x-x')$$
$$[\Phi_{m\sigma R}(x), \Phi_{m'\sigma' L}(x')] = i\pi\delta_{mm'}\delta_{\sigma\sigma'}.$$
$$(A2)$$

The Majorana fermions take care of the fermionic properties and obey anti-commutation relations

$$\{\eta_{m\sigma}, \eta_{m'\sigma'}\} = 2\delta_{mm'}\delta_{\sigma\sigma'}. \quad (A3)$$

A more convenient representation is given by the non-chiral fields,

$$\phi_{m\sigma}, \theta_{m\sigma} = \frac{1}{2}(\Phi_{m\sigma L} \pm \Phi_{m\sigma R}). \quad (A4)$$

They are connected to density and current as $\nabla\phi \propto n$ and $\nabla\theta \propto j$, and satisfy commutation relations,

$$[\phi_{m\sigma}(x), \phi_{m'\sigma'}(x')] = [\theta_{m\sigma}(x), \theta_{m'\sigma'}(x')] = 0$$
$$[\phi_{m\sigma}(x), \theta_{m'\sigma'}(x')] = i\pi\delta_{mm'}\delta_{\sigma\sigma'}\Theta(x'-x),$$
$$(A5)$$

where $\Theta(x)$ is the Heaviside step function. Finally we move to different combinations of these fields,

$$\begin{bmatrix}\phi_{c0}\\\phi_{c\pi}\\\phi_{s0}\\\phi_{s\pi}\end{bmatrix} = \frac{1}{2}\begin{bmatrix}1&1&1&1\\1&1&-1&-1\\1&-1&1&-1\\1&-1&-1&1\end{bmatrix}\begin{bmatrix}\phi_{A\uparrow}\\\phi_{A\downarrow}\\\phi_{B\uparrow}\\\phi_{B\downarrow}\end{bmatrix}, \quad (A6)$$

where $\mu = (c,s)$ represents charge and spin modes, and $\nu = (0,\pi)$ gives bonding/antibonding basis. θ's are transformed in the same manner.

The sign of each coupling constant is determined by Klein factors, and by a commutator between different chirality, $[\Phi_{R,n}(x), \Phi_{L,n'}(x')] = i\pi\delta_{n,n'}$. The eigenvalues of Klein factors composed of two Majorana fermions (different from the ones introduced for refermionization) are taken to be

$$i = \eta_{As}\eta_{Bs} = \eta_{A\uparrow}\eta_{A\downarrow}$$
$$= \eta_{A\uparrow}\eta_{B\downarrow} = \eta_{B\uparrow}\eta_{A\downarrow} = -\eta_{B\uparrow}\eta_{B\downarrow}. \quad (A7)$$

Appendix B: RG equations for unequal velocities

When two Fermi velocities are different, it is more convenient to use current operators than using refermionization. We follow the notation of Ref. 7 with slight modification:

$$J_{mr} = \sum_{ss'}\psi^\dagger_{msr}\psi_{ms'r}, \quad \boldsymbol{J}_{mr} = \sum_{ss'}\psi^\dagger_{msr}\boldsymbol{\sigma}_{ss'}\psi_{ms'r} \quad (B1)$$

$$L_r = \sum_{ss'}\psi^\dagger_{Asr}\psi_{Bs'r}, \quad \boldsymbol{L}_r = \sum_{ss'}\psi^\dagger_{Asr}\boldsymbol{\sigma}_{ss'}\psi_{Bs'r} \quad (B2)$$

$$M_{mr} = -i\psi_{m\uparrow r}\psi_{m\downarrow r}, \quad N_{rss'} = \psi_{rAs}\psi_{rBs'}. \quad (B3)$$

When $k_A \neq k_B$, the interactions terms are given by,

$$-\mathcal{H}_{\mathrm{int}} = \widetilde{g}_{1\rho}J_{AR}J_{AL} + \widetilde{g}_{1\sigma}\boldsymbol{J}_{AR}\cdot\boldsymbol{J}_{AL}$$
$$+ \widetilde{g}_{2\rho}J_{BR}J_{BL} + \widetilde{g}_{2\sigma}\boldsymbol{J}_{BR}\cdot\boldsymbol{J}_{BL}$$
$$+ \widetilde{g}_{x\rho}(J_{AR}J_{BL} + J_{BR}J_{AL}) \quad (B4)$$
$$+ \widetilde{g}_{x\sigma}(\boldsymbol{J}_{AR}\cdot\boldsymbol{J}_{BL} + \boldsymbol{J}_{BR}\cdot\boldsymbol{J}_{AL})$$
$$+ \widetilde{g}_{t\rho}(L_R L_L + \mathrm{h.c.}) + \widetilde{g}_{t\sigma}(\boldsymbol{L}_R\cdot\boldsymbol{L}_L + \mathrm{h.c.}).$$

This expression is formally the same as the one given in Ref. 7. When $k_A = k_B$, we have additional processes,

$$-\mathcal{H}'_{\mathrm{int}} = \widetilde{g}_{a\rho}\left(L_R L_L^\dagger + \mathrm{h.c.}\right) + \widetilde{g}_{a\sigma}\left(\boldsymbol{L}_R\cdot\boldsymbol{L}_L^\dagger + \mathrm{h.c.}\right). \quad (B5)$$

Umklapp processes are allowed when the filling is commensurate ($n = 2$):

$$-\mathcal{H}''_{\mathrm{int}} = \widetilde{g}_{1u}\left(M_{AR}M_{AL}^\dagger + \mathrm{h.c.}\right)$$
$$+ \widetilde{g}_{2u}\left(M_{BR}M_{BL}^\dagger + \mathrm{h.c.}\right)$$
$$+ \widetilde{g}_{xu}\left(M_{AR}M_{BL}^\dagger + M_{BR}M_{AL}^\dagger + \mathrm{h.c.}\right) \quad (B6)$$
$$+ \widetilde{g}_{tu\rho}\left(N_{R\alpha\beta}^\dagger N_{L\alpha\beta} - N_{R\alpha\beta}^\dagger N_{L\beta\alpha} + \mathrm{h.c.}\right)$$
$$+ \widetilde{g}_{tu\sigma}\left(N_{R\alpha\beta}^\dagger N_{L\alpha\beta} + N_{R\alpha\beta}^\dagger N_{L\beta\alpha} + \mathrm{h.c.}\right).$$

The $\widetilde{g}_{1u}$ and $\widetilde{g}_{2u}$ processes are allowed only when each band has commensurate filling, i.e., $k_m = \pi/2$. We ignore all the chiral scattering processes, since they only renormalize the velocities.

In the following, we use the renormalized coupling constants, $y_i = \widetilde{g}_i \pi^{-1}(v_A+v_B)^{-1}$. The RG equations for the $k_A = k_B = \pi/2$ case are

$$
\begin{aligned}
\dot{y}_{1\rho} &= -\beta \left(y_{a\rho}^2 + 3y_{a\sigma}^2 + 3y_{tu\sigma}^2 + y_{tu\rho}^2 - y_{t\rho}^2 - 3y_{t\sigma}^2\right) - \alpha y_{1u}^2 \\
\dot{y}_{2\rho} &= -\alpha \left(y_{a\rho}^2 + 3y_{a\sigma}^2 + 3y_{tu\sigma}^2 + y_{tu\rho}^2 - y_{t\rho}^2 - 3y_{t\sigma}^2\right) - \beta y_{2u}^2 \\
\dot{y}_{x\rho} &= y_{a\rho}^2 + 3y_{a\sigma}^2 - 3y_{tu\sigma}^2 - y_{tu\rho}^2 - y_{t\rho}^2 - 3y_{t\sigma}^2 - y_{xu}^2
\end{aligned}
\tag{B7}
$$

$$
\begin{aligned}
\dot{y}_{1\sigma} &= -2\beta \left(y_{a\sigma}\left(y_{a\sigma} + y_{a\rho}\right) + y_{tu\sigma}\left(y_{tu\sigma} + y_{tu\rho}\right) + y_{t\sigma}\left(y_{t\sigma} - y_{t\rho}\right)\right) - 4\alpha y_{1\sigma}^2 \\
\dot{y}_{2\sigma} &= -2\alpha \left(y_{a\sigma}\left(y_{a\sigma} + y_{a\rho}\right) + y_{tu\sigma}\left(y_{tu\sigma} + y_{tu\rho}\right) + y_{t\sigma}\left(y_{t\sigma} - y_{t\rho}\right)\right) - 4\beta y_{2\sigma}^2 \\
\dot{y}_{x\sigma} &= -2 \left(y_{a\sigma}\left(y_{a\sigma} - y_{a\rho}\right) + y_{tu\sigma}\left(y_{tu\sigma} - y_{tu\rho}\right) + y_{t\sigma}\left(y_{t\sigma} + y_{t\rho}\right)\right) - 4y_{x\sigma}^2
\end{aligned}
\tag{B8}
$$

$$
\begin{aligned}
\dot{y}_{t\rho} &= -2y_{tu\rho}y_{xu} + y_{t\rho}y_{c-} + 3y_{t\sigma}y_{s-} \\
\dot{y}_{t\sigma} &= 2y_{tu\sigma}y_{xu} + y_{t\rho}y_{s-} + y_{t\sigma}\left(y_{c-} - 2y_{s+}\right)
\end{aligned}
\tag{B9}
$$

$$
\begin{aligned}
\dot{y}_{a\rho} &= -y_{tu\rho}\left(\alpha y_{1u} + \beta y_{2u}\right) - y_{a\rho}y_{c-} - 3y_{a\sigma}y_{s-} \\
\dot{y}_{a\sigma} &= -y_{tu\sigma}\left(\alpha y_{1u} + \beta y_{2u}\right) - y_{a\rho}y_{s-} - y_{a\sigma}\left(y_{c-} + 2y_{s+}\right)
\end{aligned}
\tag{B10}
$$

$$
\begin{aligned}
\dot{y}_{1u} &= -4 \left(3\beta y_{a\sigma}y_{tu\sigma} + \beta y_{a\rho}y_{tu\rho} + \alpha y_{1u}y_{1\rho}\right) \\
\dot{y}_{2u} &= -4 \left(3\alpha y_{a\sigma}y_{tu\sigma} + \alpha y_{a\rho}y_{tu\rho} + \beta y_{2u}y_{2\rho}\right) \\
\dot{y}_{xu} &= 4 \left(3y_{t\sigma}y_{tu\sigma} - y_{t\rho}y_{tu\rho} - y_{xu}y_{x\rho}\right)
\end{aligned}
\tag{B11}
$$

$$
\begin{aligned}
\dot{y}_{tu\rho} &= -y_{a\rho}\left(\alpha y_{1u} + \beta y_{2u}\right) - 2y_{t\rho}y_{xu} - y_{tu\rho}y_{c+} - 3y_{tu\sigma}y_{s-} \\
\dot{y}_{tu\sigma} &= -y_{a\sigma}\left(\alpha y_{1u} + \beta y_{2u}\right) + 2y_{t\sigma}y_{xu} - y_{tu\rho}y_{s-} - y_{tu\sigma}\left(y_{c+} + 2y_{s+}\right),
\end{aligned}
\tag{B12}
$$

where we defined $y_{c(s)\pm} = \alpha y_{1\rho(\sigma)} + \beta y_{2\rho(\sigma)} \pm 2y_{x\rho(\sigma)}$ with $\alpha = (v_A + v_B)/(2v_A)$, and $\beta = (v_A + v_B)/(2v_B)$. For doped cases, and $k_A \neq k_B$ cases, the coupling constants which are not allowed by momentum conservation should be removed.

As we mentioned, the asymptotic behavior of a RG flow is captured by the ansatz (55), and now the ratios of coupling constants at fixed points depend on velocity differences. However, we can easily distinguish phases with different fixed point structure by looking at the signs of relevant couplings, and irrelevant couplings. In that sense, we identify phases as the same ones when the relevant couplings and the signs are the same. When the relevant couplings are different, or the signs of renormalized couplings are different, we regard them as different phases.

[*] okamoto@phys.columbia.edu

[†] millis@phys.columbia.edu

[1] C. M. Varma and A. Zawadowski, Phys. Rev. B **32**, 7399 (1985).

[2] S. P. Strong and A. J. Millis, Phys. Rev. B **50**, 9911 (1994).

[3] S. Fujimoto and N. Kawakami, J. Phys. Soc. Jpn. **63**, 4322 (1994).

[4] M. Fabrizio, A. Parola, and E. Tosatti, Phys. Rev. B **46**, 3159 (1992).

[5] A. M. Finkelstein and A. I. Larkin, Phys. Rev. B **47**, 10461 (1993).

[6] D. V. Khveshchenko and T. M. Rice, Phys. Rev. B **50**, 252 (1994).

[7] L. Balents and M. P. A. Fisher, Phys. Rev. B **53**, 12133 (1996).

[8] H. J. Schulz, Phys. Rev. B **53**, 2959 (1996).

[9] D. G. Shelton and A. M. Tsvelik, Phys. Rev. B **53**, 14036 (1996).

[10] H. H. Lin, L. Balents, and M. P. A. Fisher, Phys. Rev. B **58**, 1794 (1998).

[11] S. Lee, J. B. Marston, and J. O. Fjaerestad, Phys. Rev. B **72**, 075126 (2005).

[12] P. Chudzinski, M. Gabay, and T. Giamarchi, Phys. Rev. B **78**, , 075124 (2008).

[13] D. G. Shelton, A. A. Nersesyan, and A. M. Tsvelik, Phys. Rev. B **53**, 8521 (1996).

[14] E. H. Kim, G. Fáth, J. Sólyom,and D. J. Scalapino, Phys. Rev. B **62**, 14965 (2000).

[15] P. Azaria, A. O Gogolin, P. Lecheminant, and A. A. Nersesyan, Phys. Rev. Lett. **83**, 624 (1999).

[16] M. Tsuchiizu and A. Furusaki, Phys. Rev. B **66**, 245106 (2002).

[17] C. Wu, W. V. Liu, and E. Fradkin, Phys. Rev. B **68**, 115104 (2003).

[18] S. Wang, M. B. Yilmaz, K. R. Knox, N. Zaki, J. I. Dadap, R. M. Osgood, T. Valla, and P. D. Johnson, Phys. Rev. B **77**, 115448 (2008).

[19] N. Zaki, D. Potapenko, P. D. Johnson, and R. M. Osgood, Phys. Rev. B **80**, 155419 (2009).

[20] R. M. Konik, H. Saleur, and A. W. W. Ludwig, Phys. Rev. B **66**, 075105 (2002).

[21] D. Controzzi and A. M. Tsvelik, Phys. Rev. B **72**, 035110 (2005).

[22] T. Momoi and T. Hikihara, Phys. Rev. Lett. **91**, 256405 (2003).

[23] E. Boulat, P. Azaria, and P. Lecheminant, Nucl. Phys. B **822**, 367 (2009).

[24] H. Nonne, E. Boulat, S. Capponi, and P. Lecheminant, Phys. Rev. B **82**, 155134 (2010).

[25] H. Kramers and G. Wannier, Phys. Rev. **60**, 252 (1941).

[26] A. M. Tsvelik, Phys. Rev. B **83**, 104405 (2011).

[27] P. Gambardella, A. Dallmeyer, K. Maiti, M. C. Malagoli, W. Eberhardt, K. Kern, and C. Carbone, Nature **416**, 301 (2002).

[28] A. Koga, N. Kawakami, T. M. Rice, and M. Sigrist, Phys. Rev. Lett. **92**, 216402 (2004).

[29] J. Okamoto and A. J. Millis, Phys. Rev. B **84**, 205433 (2011).

[30] H. C. Lee, P. Azaria, and E. Boulat, Phys. Rev. B **69**, 155109 (2004).

[31] J. Voit, Rep. Prog. Phys. **58**, 977 (1995).

[32] T. Giamarchi, *Quantum physics in one dimension* (Clarendon, 2004).

[33] A. O. Gogolin, A. A. Nersesyan, and A. M. Tsvelik, *Bosonization and strongly correlated systems* (Cambridge University Press, 2004).

[34] Y. Nishiyama, N. Hatano, and M. Suzuki, J. Phys. Soc. Jpn. **64**, 1967 (1995).

[35] I. Affleck, T. Kennedy, E. H. Lieb, and H. Tasaki, Phys. Rev. Lett. **59**, 799 (1987).

[36] M. Nakamura, Physica B **329-333**, 1000 (2003).

[37] R. Assaraf, P. Azaria, E. Boulat, M. Caffarel, and P. Lecheminant, Phys. Rev. Lett. **93**, 016407 (2004).

[38] J. E. Bunder and H. H. Lin, Phys. Rev. B **75**, 075418 (2007).

[Note1] To get the same form, we have to redefine $\psi_L^{c\pi} = \left(\xi_L^5 - i\xi_L^6\right)/\sqrt{2}$. Here the modes correspond to the new orbital part are ξ_5 and ξ_6, and the Ising mode is carried by ξ_4.

[40] D. Gross and A. Neveu, Phys. Rev. D **10**, 3235 (1974).

[41] R. Shankar, Phys. Rev. Lett. **55**, 453 (1985).

[42] J. L. Cardy, *Scaling and renormalization in statistical physics* (Cambridge University Press, 1996).

[43] J. von Delft and H. Schoeller, Annalen der Physik **7**, 225 (1998).

[44] W. Chen, M. S. Chang, H. H. Lin, D. Chang and C. Y. Mou, Phys. Rev. B **70**, 205413 (2004).

[45] A. Zamolodchikov, JETP Lett **43**, 9 (1986).

[46] M. Nakamura, Phys. Rev. B **61**, 16377 (2000).

[47] M. Tsuchiizu and A. Furusaki, Phys. Rev. Lett. **88**, 056402 (2002).

[48] K. Kugel and D. Khomskii, JETP Lett. **15**, 446 (1972).

[49] M. Cyrot and C. Lyon-Caen, J. Phys. (Paris) **36**, 253 (1975).

[50] W. Gill and D. J. Scalapino, Phys. Rev. B **35**, 215 (1987).

[51] H. Sakamoto, T. Momoi, and K. Kubo, Phys. Rev. B **65**, 224403 (2002).

[52] N. Zaki (private communication).

[53] D. Carpentier and E. Orignac, Phys. Rev. B **74**, 085409 (2006).